

# Characteristic, completion or matching timescales? An analysis of temporary boundaries in enzyme kinetics

Justin Eilertsen<sup>a</sup>, Wylie Stroberg<sup>a</sup>, Santiago Schnell<sup>a,b,1</sup>

<sup>a</sup>*Department of Molecular & Integrative Physiology, University of Michigan Medical School, Ann Arbor, MI 48109, USA*

<sup>b</sup>*Department of Computational Medicine & Bioinformatics, University of Michigan Medical School, Ann Arbor, MI 48109, USA*

---

## Abstract

Scaling analysis exploiting timescale separation has been one of the most important techniques in the quantitative analysis of nonlinear dynamical systems in mathematical and theoretical biology. In the case of enzyme catalyzed reaction, it is often overlooked that the characteristic timescales used for the scaling of reaction rates are not ideal for determining when concentrations and production rates reach their maximum values. In this work, we first illustrate this point by considering the classic example of the single-enzyme, single-substrate Michaelis–Menten reaction mechanism. We then extend this analysis to a more complicated reaction mechanism, the auxiliary enzyme reaction, in which a substrate is converted to product in two sequential enzyme-catalyzed reactions. In this case, depending on the ordering of the relevant timescales, either two or three dynamic regimes can emerge. In addition to the characteristic timescales for these regimes, we derive matching timescales that precisely determine when the transitions from initial fast transient to steady-state kinetics occurs. The approach presented here is applicable to a wide range of singular perturbation problems in nonlinear dynamical systems.

*Keywords:* Timescales, Chemical kinetics, Slow and fast dynamics, Perturbation methods, Enzyme kinetics, Nonlinear dynamical systems

---

*Email address:* [schnells@umich.edu](mailto:schnells@umich.edu) (Santiago Schnell)

<sup>1</sup>Corresponding author

## 1. Introduction

Nonlinear differential equations are used to model the dynamical behavior of natural phenomena in science. As the natural phenomena becomes more complex, the dynamics is influenced by multiple timescales, which create technical problems in the mathematical analysis and numerical computation of models (Lin and Segel, 1988).

The 21st century has been dominated by advances in the biological and biomedical sciences. As a result, examples of complex dynamical systems have become ubiquitous in theoretical and mathematical biology. Despite their complexity, all major levels of biological organization have one common dynamical denominator: chemical reactions are continuously taking places in organelles, cells, tissues, organs, organ systems, organisms, populations, communities, ecosystem, and biosphere. Most of these reactions involve enzymes. Arguably, if biology is to be understood as a dynamical process, enzyme catalyzed reactions need to be investigated quantitatively (Gallagher, 2004).

The quantitative description of any enzyme catalyzed chemical reaction is often decomposed into two categories: thermodynamics and kinetics. The former tells us if a particular reaction is favorable, while latter describes the timescales over which reactions occur. From the point of view of the experimental scientist, chemical kinetics focuses on the measurement of concentrations as a function of time with the goal of characterizing reaction properties (Espenson, 1995). Regardless of whether a kinetic model is linear or nonlinear, stochastic or deterministic, the effectiveness of the model is only as good as the timescales it predicts (Shoffner and Schnell, 2017): timescales provide not only an estimation of the effective duration of the reaction, but are also critical in characterizing reaction mechanisms. This topic is not unfamiliar to Philip K. Maini, who has worked in a number of diverse areas of mathematical biology, including enzyme kinetics (Frenzen and Maini, 1988; Burke et al., 1990, 1993; Schnell and Maini, 2000, 2002, 2003).

Philip K. Maini mentored one of us, Santiago Schnell, through the rigorous theory of timescale analysis in chemical kinetics that lies at the intersection of chemistry and geometric singular perturbation theory (GSPT). In fact, GSPT is widely applicable not only to chemical kinetics, but to a plethora of important biological models (Bertram and Rubin, 2017). Largely,

GSPT is the study of dynamical systems of the form

$$\dot{x} = f(x, y), \tag{1a}$$

$$\varepsilon \dot{y} = g(x, y), \tag{1b}$$

where  $\varepsilon \ll 1$  and “ $\cdot$ ” denotes differentiation with respect to time; such systems are often referred to as a slow/fast systems, since changes in the variable  $x$  occur over timescales that are large compared to the timescales over which the variable  $y$  changes. For example, if time is rescaled as  $t_\varepsilon = t/\varepsilon$ , then the evolution of (1) becomes

$$x' = \varepsilon f(x, y), \tag{2a}$$

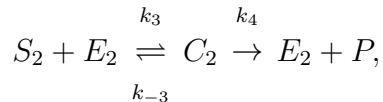
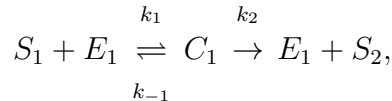
$$y' = g(x, y), \tag{2b}$$

with “ $'$ ” denoting differentiation with respect to  $t_\varepsilon$ . Over the  $t_\varepsilon$ -timescale, the variable  $x$  barely changes, while the variable  $y$  can change significantly. In contrast, the change in variable  $x$  is nontrivial over the  $t$ -timescale and, due to the presence of slow manifolds (Roussel and Fraser, 1990), the change in the variable  $y$  can be shown to be explicitly dependent on change in  $x$ . Thus, the dynamics of (1) is dependent on two different timescales: the fast timescale,  $t_\varepsilon$ , and the slow timescale,  $t$ . Each timescale defines a unique dynamical regime: the initial, “ $t_\varepsilon$ -regime”, over which  $x$  is essentially constant and  $y$  changes rapidly, and the “ $t$ -regime”, in which  $x$  changes significantly and the change in  $y$  is dictated solely by the change in  $x$ .

GSPT has a rich relationship with chemical kinetics, particularly regarding the application of *matched asymptotics*. Matched asymptotics is a common mathematical approach aimed at finding an accurate approximation to the solution to an equation, or system of equations (see Kuehn, 2015, for an excellent discussion on matched asymptotics). Usually, the study of matched asymptotics is linked to singular perturbation problems that arise as a consequence of underlying disparate spatial layers, such as boundary layers that form in pattern formation during embryonic development (see Maini et al., 2012). The specific aim of matched asymptotics is to generate a *composite solution*, which is constructed by gluing together local solutions (solutions that are asymptotically valid on different regimes) to comprise a solution that is uniformly valid (Holmes, 2013). Of principal interest in chemical kinetics, for which there typically exist multiple disparate timescales, is to determine the timescales that contribute to the composite solution.

In this work, we begin by introducing the characteristic timescale, which is a well-defined timescale from dynamical systems theory. We show that the established “fast timescale” of the single-enzyme, single-substrate, Michaelis–Menten (MM) reaction mechanism is in fact a characteristic timescale, and we demonstrate that characteristic timescales are the correct timescales for constructing the composite solution. However, we also show that characteristic timescales are not suitable for determining precisely *when* a transition from one dynamical regime to another dynamical regime occurs; this means that characteristic timescales cannot tell us when exactly concentrations of certain chemical species reach their peak values, or precisely when the rate of product generation reaches its maximum value. Thus, there is a need for an additional timescale, which we refer to as a *matching timescale*, that provides an accurate temporal boundary between specific dynamic (kinetic) regimes. Its derivation follows directly from the theory of GSTP and matched asymptotics, and we demonstrate that appropriate matching timescales can be constructed from physical knowledge of the characteristic timescales. Specifically, through the application of Tikhonov–Fenichel Theory, we derive the correct matching timescale for the MM reaction mechanism, and show that it can be explicitly obtained from the fast and slow characteristic timescales. We also categorize the corresponding slow timescale of the MM reaction mechanism as either a characteristic, depletion, or completion timescale.

Most chemical reactions that consist of two disparate timescales are well-understood; however, much of the modern employment of GSPT consists of analyzing problems that are comprised of *more* than two timescales Nan et al. (2015); Letson et al. (2017); Vo et al. (2013), and it is time to push enzyme kinetics in this direction. Thus, we analyze the kinetics of the auxiliary enzyme reaction mechanism Eilertsen and Schnell (2018)



under the assumption that the auxiliary enzyme,  $E_2$ , is in excess. We show that the dynamics of this reaction can consist of three regimes, in which case

there are four relevant timescales. We illustrate that different orderings of the timescales must be considered in order to establish a complete description of the kinetics. The relevant characteristic timescales that approximate the duration of each regime are derived through geometric analysis of the phase-plane. Lastly, composite solutions and precise matching timescales are obtained.

## 2. The characteristic timescale

Consider a general, autonomous dynamical system of the form

$$\dot{x} = f(x), \quad (3)$$

and suppose  $f(x)$  has a fixed point,  $x^*$ , such that  $f(x^*) = 0$ . The *characteristic timescale* is reciprocal of the exponential growth/decay rate of the linearized equation in a small neighborhood surrounding  $x^*$ . That is, if  $\delta$  is a small perturbation, then

$$f(x^* + \delta) \simeq \left. \frac{df}{dx} \right|_{x=x^*} \delta \equiv f'(x^*)\delta, \quad (4)$$

and therefore

$$\dot{\delta} \simeq f'(x^*)\delta. \quad (5)$$

Since linearized evolution of the perturbation grows or decays according to

$$\delta \simeq \exp[f'(x^*)t], \quad (6)$$

the characteristic timescale,  $t_\chi$ , is the time required for the perturbation to *significantly* grow or decay:

$$t_\chi = \frac{1}{|f'(x^*)|}. \quad (7)$$

For a linear, exponential decay differential equation of the form

$$\dot{x} = -\gamma x, \quad x(0) = x_0, \quad (8)$$

the characteristic timescale is  $1/\gamma$ , and corresponds to the exact amount of time it takes the initial condition to decay to

$$x(t_\chi) = (1 - \ell)x_0, \quad \ell = \frac{\exp(1) - 1}{\exp(1)}, \quad (9)$$

which is roughly  $0.37x_0$ . In addition, for a linear equation of the form

$$\dot{x} = -\gamma x + A, \quad x(0) = 0, \quad (10)$$

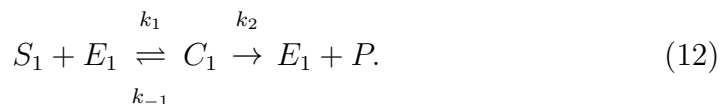
where  $A$  is a constant, the characteristic timescale,  $1/\gamma$ , is the exact amount of time it takes  $x$  to grow to

$$x(t_\chi) = \ell \frac{A}{\gamma} \equiv \ell x^{\max}, \quad (11)$$

or roughly  $0.63x^{\max}$ .

### 3. The slow and fast timescales of the Michaelis–Menten reaction mechanism: An exercise in the power and limitations of characteristic timescales

We continue by reviewing the pertinent characteristic timescales for the well-studied single-enzyme, single-substrate reaction in which an enzyme,  $E_1$ , binds to a substrate,  $S_1$  (forming an intermediate enzyme-substrate complex,  $C_1$ ), and catalyzes the conversion of  $S_1$  into product,  $P$ :



The kinetics of the reaction depend not only in the rate constants,  $k_1$  and  $k_{-1}$ , and the catalytic constant  $k_2$ , but also on the initial concentrations of  $S_1$  and  $E_1$ . Specifically, the *reduced* mass action equations that govern the kinetics of (12) are

$$\dot{s}_1 = -k_1(e_1^0 - c_1)s_1 + k_{-1}c_1, \quad (13a)$$

$$\dot{c}_1 = k_1(e_1^0 - c_1)s_1 - (k_{-1} + k_2)c_1, \quad (13b)$$

where  $s_1$  and  $c_1$  denote the concentrations of  $S_1$  and  $C_1$ , respectively, and  $e_1^0$  is the initial concentration of  $E_1$ . We will assume that the reaction consists of only an initial enzyme concentration,  $e_1^0$ , and an initial substrate concentration,  $s_1^0$ , when  $t = 0$ .

### 3.1. The characteristic initial fast transient of the reaction

It is well-established that, under the reactant stationary assumption (RSA) (Hanson and Schnell, 2008; Schnell, 2014), the dynamics of (12) initialize with a brief initial transient during which the intermediate complex concentration,  $c_1$ , accumulates rapidly towards its maximum, and the substrate  $s_1$  remains effectively unchanged from the initial substrate concentration  $s_1^0$ . The RSA ensures  $s_1 \approx s_1^0$  during the initial transient of the reaction. Under the RSA, equation (13b) is approximately

$$\dot{c}_1 \simeq k_1(e_1^0 - c_1)s_1^0 - (k_{-1} + k_2)c_1, \quad (14)$$

which admits the solution

$$c_1 \simeq c_1^{\max}(1 - \exp[-k_1(K_{M_1} + s_1^0)t]), \quad c_1^{\max} = \frac{e_1^0 s_1^0}{K_{M_1} + s_1^0}. \quad (15)$$

In the above equation,  $K_{M_1} = (k_{-1} + k_2)/k_1$  is the Michaelis constant. The characteristic timescale of the intermediate complex species that arises from (15) is  $t_{c_1}$ :

$$t_{c_1} = \frac{1}{k_1(K_{M_1} + s_1^0)}. \quad (16)$$

Technical justification for  $t_{c_1}$  was originally obtained (Segel, 1988; Segel and Slemrod, 1989) through scaling analysis: introducing the dimensionless parameters

$$\sigma_1 \equiv \frac{s_1^0}{K_{M_1}}, \quad \kappa_1 \equiv k_{-1}/k_1, \quad \beta_1 \equiv \frac{1}{1 + \sigma_1} < 1, \quad \alpha_1 \equiv \frac{\kappa_1}{1 + \kappa_1} < 1, \quad (17)$$

allows equations (13a)–(13b) to be rescaled into their dimensionless form

$$\begin{aligned} \frac{d\hat{s}_1}{d\tau} &= \varepsilon_1 [-\hat{s}_1 + (1 - \beta_1)\hat{c}_1\hat{s}_1 + \beta_1\alpha_1\hat{c}_1], & \varepsilon_1 &= \frac{e_1^0}{K_{M_1} + s_1^0} \\ \frac{d\hat{c}_1}{d\tau} &= \hat{s}_1 - (1 - \beta_1)\hat{c}_1\hat{s}_1 - \beta_1\hat{c}_1, \end{aligned} \quad (18)$$

where  $\tau = t/t_{c_1}$ ,  $\hat{s}_1 = s_1/s_1^0$  and  $\hat{c}_1 = c_1/c_1^{\max}$ . It is clear from (18) that if  $\varepsilon_1 \ll 1$ , then  $s_1 \simeq s_1^0$  when  $t \leq t_{c_1}$ . Formally, the qualifier  $\varepsilon_1 \ll 1$  is the condition for RSA, and  $t_{c_1}$  is the *characteristic* timescale of the initial fast transient.

### 3.2. The slow timescale of the reaction: from characteristic to completion

In contrast to the brief timescale over which  $c_1$  accumulates (i.e.  $t_{c_1}$ ),  $s_1$  changes over a much longer timescale. The timescale over which there is appreciable change in  $s_1$  is the slow timescale of the reaction or the substrate depletion timescale. As a direct result from singular perturbation theory, the depletion of  $s_1$  is approximately

$$\dot{s}_1 \simeq -\frac{V_1}{K_{M_1} + s_1}s_1 \quad (19)$$

after the initial fast transient (i.e. for  $t > t_{c_1}$ ). The above expression is known as the MM equation, where  $V_1 = k_2 e_1^0$  is the limiting rate of the reaction. The slow timescale,  $t_{s_1}$ , is given by

$$t_{s_1} = \frac{s_1^0}{\max|\dot{s}_1|} = \frac{K_{M_1} + s_1^0}{V_1}. \quad (20)$$

The technical justification of (20) is acquired through scaling analysis. By writing the dimensionless form (13a)–(13b) with respect to  $T = t/t_{s_1}$  yields

$$\begin{aligned} \frac{d\hat{s}_1}{dT} &= (1 + \kappa_1)(1 + \sigma_1) [-\hat{s}_1 + (1 - \beta_1)\hat{c}_1\hat{s}_1 + \beta_1\alpha_1\hat{c}_1], \\ \varepsilon_2 \frac{d\hat{c}_1}{dT} &= \hat{s}_1 - (1 - \beta_1)\hat{c}_1\hat{s}_1 - \beta_1\hat{c}_1. \end{aligned} \quad (21)$$

The dimensionless parameter,  $\varepsilon_2$ , is the ratio of fast and slow timescales:  $\varepsilon_2 = t_{c_1}/t_{s_1}$ .

The MM equation (19) admits a closed-form solution

$$s_1 = K_{M_1} W[\sigma_1 \exp(\sigma_1 - \eta_1 t)], \quad \eta_1 = \frac{V_1}{K_{M_1}}, \quad (22)$$

where  $W[\cdot]$  is the Lambert- $W$  function (Schnell and Mendoza, 1997). This closed form solution is known as the Schnell-Mendoza equation (Clark et al., 2011; Feng et al., 2014; Son et al., 2015; Murugan, 2018). While mathematicians typically refer to  $t_{s_1}$  as the slow timescale, the chemical interpretation of  $t_{s_1}$  depends on the specific initial concentration,  $\sigma_1$ . If  $\sigma_1 \ll 1$ , then (22) is asymptotic to

$$s_1 \simeq s_1^0 \exp(\sigma_1 - \eta_1 t). \quad (23)$$



Consequently, we obtain:

$$s_1(t_{s_1}) \simeq (1 - \ell)s_1^0. \quad (24)$$

Thus, if the initial substrate concentration is much less than the Michaelis constant,  $K_{M_1}$ , then the slow timescale,  $t_{s_1}$ , is a *characteristic timescale* for the substrate species.

The calculus of the Lambert- $W$  function determines the relevant chemical interpretation of  $t_{s_1}$  as  $\sigma_1$  increases. When  $t = t_{s_1}$ , the substrate concentration is identically  $K_{M_1}W[(1 - \ell)\sigma_1]$ . Furthermore, treating (22) as exact and noting

$$\frac{d}{du} \left( u - W[u] \right) > 0, \quad u > 0, \quad (25)$$

we see that  $(1 - \ell)s_1^0$  is actually a supremum:

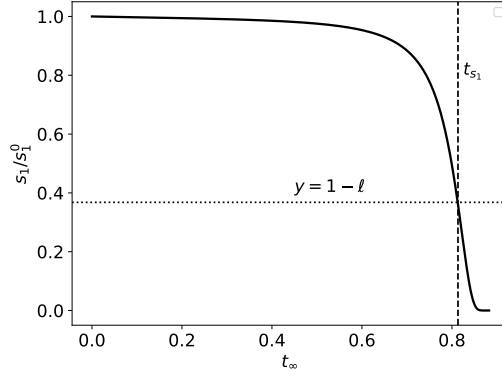
$$\sup (s_1(t_{s_1})) = (1 - \ell)s_1^0. \quad (26)$$

Furthermore, it follows from (25) that if  $\sigma_1 \gg 1$ , then

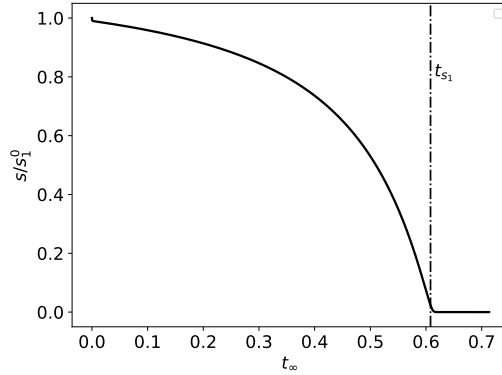
$$s_1(t_{s_1}) = K_{M_1}W[(1 - \ell)\sigma_1] \ll (1 - \ell)s_1^0, \quad (27)$$

in which case we categorize  $t_{s_1}$  as a *completion timescale*, since it is proportional to the total length of the reaction (see FIGURES 1a and 1b).

In the intermediate range, when  $\sigma_1$  is neither  $\sigma_1 \ll 1$  or  $\sigma_1 \gg 1$ ,  $t_{s_1}$  is still the appropriate timescale over which a *significant* reduction in substrate concentration occurs, and in this case we refer to the slow timescale as the *depletion timescale*, since it is too long to be a characteristic timescale, but too short to be a completion timescale.



(a)



(b)

Figure 1: **The graphical illustrations of the characteristic and completion timescales for the Michaelis–Menten reaction mechanism (12).** When  $\sigma_1 \ll 1$ , the timescale  $t_{s_1}$  is the characteristic time of the substrate species [Panel (a)]. In contrast, when  $\sigma_1 \gg 1$ , the reaction is essentially complete when  $t = t_{s_1}$  [Panel (b)]. The solid black curves are numerical solutions to the mass action equations (42a)–(42b) and the vertical dashed/dotted lines correspond to  $t = t_{s_1}$ . The dotted horizontal line corresponds to the scaled characteristic value  $(1 - \ell)s_1^0$ . In (a), the constants (without units) used in the numerical simulation are:  $e_1^0 = 1$ ,  $k_1 = 0.01$ ,  $k_2 = 10$ ,  $k_{-1} = 1$  and  $s_1^0 = 100$ . In (b), the constants (without units) used in the numerical simulation are:  $e_1^0 = 1$ ,  $k_1 = 10$ ,  $k_2 = 10$ ,  $k_{-1} = 1$  and  $s_1^0 = 100$ . Time has been mapped to the  $t_\infty$  scale:  $t_\infty(t) = 1 - 1/\ln(t + e)$ .

3.3. *Matched asymptotics: The composite solution for the time course of the reaction*

Expressing the asymptotic solution to (13a)–(13b) as,

$$\begin{cases} s_1 \simeq s_1^0, \\ c_1 \simeq c_1^{\max} \{1 - \exp[-t/t_{c_1}]\}, \end{cases} \quad t \leq t_{c_1} \quad (28a)$$

$$\begin{cases} s_1 \simeq K_{M_1} W [\sigma_1 \exp(\sigma_1 - \eta_1 t)], \\ c_1 \simeq \frac{e_1^0}{K_{M_1} + s_1} s_1, \end{cases} \quad t > t_{c_1} \quad (28b)$$

serves well to convey the fact that the dynamics of the reaction changes depending on where a particular time point falls in relation to  $t_{c_1}$ . However, equations (28a)–(28b) are misleading: there is a large transition regime surrounding  $t_{c_1}$  and, within this transition regime, the outer solution (28b) does not accurately approximate the solution (see FIGURE 2).

The presence of a transition regime does not suggest that  $t_{c_1}$  is incorrect; in fact, the timescales derived in the previous section are *the* correct timescales that categorize the fast and slow regimes of the reaction. To see why, and to mitigate the effect of the transition region, we construct the *composite solution* for the intermediate,  $c_1^{io}$ :

$$c_1^{io} = \frac{e_1^0}{K_{M_1} + s_1} s_1 - c_1^{\max} [1 - \exp(-t/t_{c_1})]. \quad (29)$$

The composite solution provides a uniform asymptotic solution that is valid for all time; furthermore, from the accuracy of the composite solution, the characteristic timescale,  $t_{c_1}$ , and the slow timescale,  $t_{s_1}$ , are consequently shown to be the *right* timescales from which to construct the composite solution (see FIGURE 3).

3.4. *The shortcoming of the characteristic timescale is that it is not a matching timescale*

From a theoretical point of view, the composite solution has little advantage over the numerical solution in terms of estimating *when* the transition

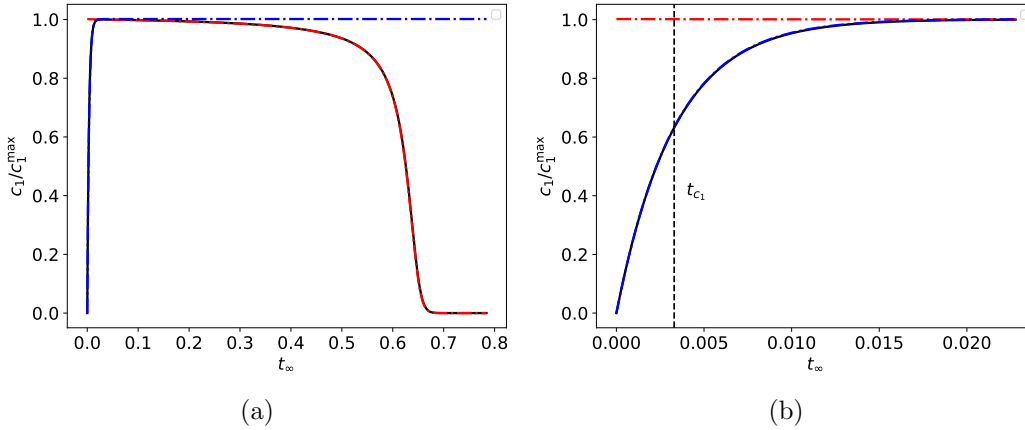


Figure 2: **Graphical illustrations of the inner and outer solutions, as well as the transition regime for the Michaelis–Menten reaction mechanism (12).** In panel (a) as  $\varepsilon_1 \rightarrow 0$ , the inner (28a) and outer (28b) solutions lay nicely over the numerical solution. The solid black curve is the numerical solution to (13a)–(13b). The dashed/dotted blue curve is the inner solution (28a), and the dashed/dotted red curve is the outer solution (28b). Panel (b) is a close-up of the transition regime in panel (a) that surrounds  $t_{c_1}$ ; notice that the outer solution does not approximate well the numerical solution when  $t_{c_1} \lesssim t$ . The initial concentrations and rate constants used in the numerical simulation are:  $k_1 = 1$ ,  $k_2 = 10$ ,  $k_{-1} = 1$ ,  $e_1^0 = 1$  and  $s_1^0 = 100$  (units have been omitted). All approximations have been scaled by their numerically–obtained maximum values, and time has been mapped to the  $t_\infty$  scale:  $t_\infty(t) = 1 - 1/\ln(t + e)$

to steady-state phase occurs. We will designate the time at which the transition occurs as a *matching timescale*; this is the time at which the inner and outer solutions become practically indistinguishable. The obvious candidate for a matching timescale is  $t_{c_1}$ . The caveat with utilizing  $t_{c_1}$  as a matching timescale is that  $t_{c_1}$  is a characteristic timescale, and hence will also provide characteristic, as opposed to limiting, values of the concentrations within a given regime. To clearly illustrate why  $t_{c_1}$  fails to be an adequate matching timescale requires some technical treatment of the underlying mathematics of the problem, and a proper analysis requires a phase–plane analysis of the mass action equations (13a)–(13b). After the initial buildup of the intermediate, the phase–plane trajectory is asymptotic to a slow manifold,  $\mathcal{M}_\varepsilon$ . The slow manifold is invariant, and is at a  $\mathcal{O}(\varepsilon_2)$ -distance from the  $c_1$ -nullcline,

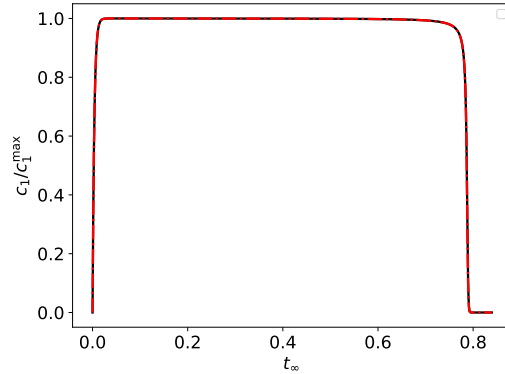


Figure 3: **A graphical comparison of the composite and numerical solutions for the time course of the Michaelis–Menten reaction (12).** As  $\varepsilon_1 \rightarrow 0$ , the composite solution lays nicely over the numerical solution. The solid black curve (barely visible) is the numerical solution to (13a)–(13b). The dashed/dotted red curve is the composite solution (29). The initial concentrations and rate constants used in the numerical simulation are:  $k_1 = 1$ ,  $k_2 = 1$ ,  $k_{-1} = 1$ ,  $e_1^0 = 1$  and  $s_1^0 = 100$  (units have been omitted). All approximations have been scaled by their numerically–obtained maximum values, and time has been mapped to the  $t_\infty$  scale:  $t_\infty(t) = 1 - 1/\ln(t + e)$ .

$\mathcal{M}_0$ :

$$\mathcal{M}_0 = \left\{ (s_1, c_1) : c_1 - \frac{e_1^0}{K_{M_1} + s_1} s_1 = 0 \right\} \quad (30)$$

The outer solution, (28a), is valid once the trajectory is *extremely close* to the slow manifold, which implies  $c_1$  should be near its maximum value at the onset of the outer solution validity. The complex reaches its maximum value once the trajectory reaches  $\mathcal{M}_0$ . However, when  $t = t_{c_1}$ , the concentration of the complex is far enough away from its maximum value to render the outer solution invalid:

$$c_1(t_{c_1}) \approx \ell c_1^{\max} < c_1^{\max}. \quad (31)$$

Thus,  $c_1(t_{c_1}) \notin \mathcal{M}_0$ , and therefore the trajectory is not quite close enough to  $\mathcal{M}_\varepsilon$  to justify (28a) as an asymptotic solution (again, see FIGURE 2).

A precise estimate of the actual time it takes  $c_1$  to reach its maximum concentration (we will denote this timescale as  $t_{c_1}^*$ ) can be obtained by either: (i) solving the mass action equations exactly or, (ii) by means of an asymptotic approximation. Employing strategy (i) is difficult due to the non-linearity of the equations; strategy (ii) tends to be more straightforward to implement. To utilize (ii), we first remark that we are immediately met with

an obvious conundrum if we try to estimate  $t_{c_1}^*$  directly from (28a) or (28b): (28a) predicts it will take an infinite amount of time for  $c_1$  to reach  $c_1^{\max}$ , while (28b) predicts  $t_{c_1}^* = 0$ . To work around this, we look for an asymptotic estimate to  $t_{c_1}^*$ , and remind ourselves that both (28a) and (28b) have been obtained under the assumption that  $\varepsilon_2 \equiv 0$ . In the asymptotic context,  $\varepsilon_2$  becomes synonymous with 0 in the limiting case. Thus, we solve

$$c_1^{\max} \left[ 1 - e^{-t/t_{c_1}} \right] = c_1^{\max} (1 - \varepsilon_2) \quad (32)$$

for  $t$  to obtain an approximation for  $t_{c_1}^*$ :

$$t_{c_1}^* \approx -t_{c_1} \ln \varepsilon_2. \quad (33)$$

The timescale (33) is the matching timescale. While not exact, the approximation (33) *is* precise, and provides a useful estimate of the exact transition from transient to steady-state kinetics for single-enzyme, single-substrate MM reaction (see FIGURES 4a and 4b).

As a final remark, we note that the asymptotic approximation (33) is not without rigorous justification. A generic fast/slow dynamical system of the form

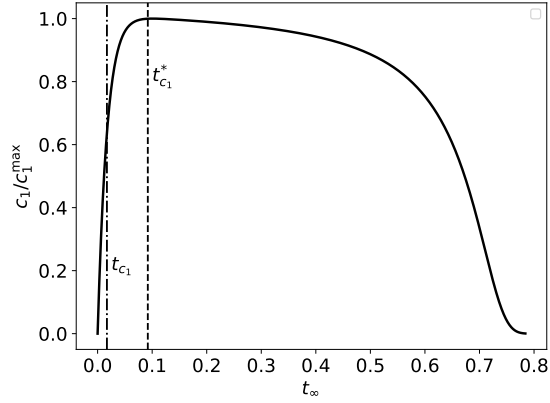
$$\dot{x} = f(x, y), \quad (34a)$$

$$\varepsilon \dot{y} = g(x, y), \quad (34b)$$

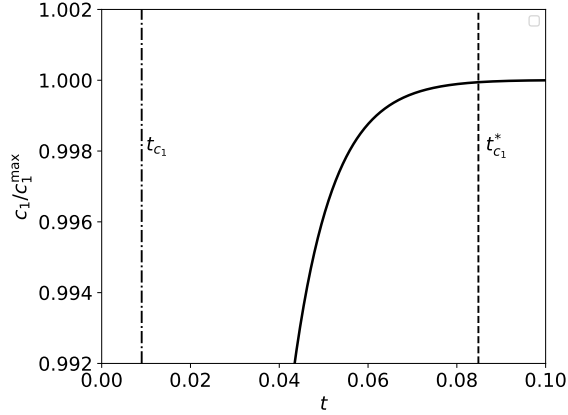
defines a corresponding slow manifold of the form  $y = h(x)$ , where  $g(x, h(x)) = 0$ ; let  $D$  be the domain over which  $h : D \rightarrow \mathbb{R}^n$  is continuous. If  $g$  and  $f$  are sufficiently smooth, then the following theorem provides a technical justification for (33):

**Theorem 1.** *Convergence towards the slow manifold: Suppose the system (34a)–(34b) has an associated slow manifold,  $\mathcal{M}_0 = \{(x, y) : y = h(x) \ \& \ x \in D\}$ , that is uniformly asymptotically stable. If  $f$ ,  $g$  and their first two derivatives are uniformly bounded in a neighborhood “ $N$ ” of  $\mathcal{M}$ , then there are positive constants  $\varepsilon_0$ ,  $b_0$ ,  $b_1$ ,  $\Lambda$ , and  $M$  such that for any initial condition  $(x_0, y_0) \in N$  such that  $\|y_0 - h(x_0)\| \leq b_0$ , and any  $\varepsilon$  such that  $0 < \varepsilon < \varepsilon_0$ , the following bound holds:*

$$\|y(t) - h(x(t))\| \leq M \|y_0 - h(x_0)\| \exp[-\Lambda t/\varepsilon] + b_1 \varepsilon. \quad (35)$$



(a)



(b)

Figure 4: **The validity of  $t_{c_1}^*$  and a graphical representation of its comparison with  $t_{c_1}$  for the Michaelis-Menten reaction mechanism (12).** In panels (a) and (b), the solid black curve is the numerically-computed solution to (42a)–(42b). The dotted/dashed vertical curve corresponds to  $t_{c_1}$ , and the dashed vertical curve corresponds to  $t_{c_1}^*$ . The initial concentrations and rate constants used in the numerical simulation are:  $k_1 = 0.1$ ,  $k_2 = 10$ ,  $k_{-1} = 1$ ,  $e_1^0 = 1$  and  $s_1^0 = 1000$  (units have been omitted). In panel (a), time has been mapped to the  $t_\infty$  scale:  $t_\infty(t) = 1 - 1/\ln(t + e)$ . Panel (b) is a closeup that illustrates the validity of  $t_{c_1}^*$ ; time is unscaled in panel (b).

The bound given by (35) will hold provided  $x(t) \in D$ . Notice the slow manifold utilized in the theorem is not defined to be *invariant*; in fact,  $\mathcal{M}_0$  is the nullcline associated with the fast variable,  $y$ , and is formally referred

to as *the critical manifold*.

What the bound specifically tells us is that if  $t = \varepsilon |\ln \varepsilon|$ , then

$$\|y(t) - h(x(t))\| \leq M \|y_0 - h(x_0)\| \varepsilon^\Lambda + b_1 \varepsilon, \quad (36)$$

and thus the phase-plane trajectory should be at a distance that is  $\mathcal{O}(\varepsilon)$  from  $\mathcal{M}_0$  when  $t = \varepsilon |\ln \varepsilon|$ , provided  $1 \lesssim \Lambda$  and  $\|y_0 - h(x_0)\|$  is  $\mathcal{O}(1)$  (see Berglund and Gentz, 2006, for details). In a fast/slow system of the form (34a)–(34b), the small parameter  $\varepsilon$  is proportional to the ratio of the fast and slow timescales. Moreover, the system (34a)–(34b) is assumed to be dimensionless; thus, if we apply Theorem (1) to

$$\begin{aligned} \frac{d\hat{s}_1}{dT} &= (1 + \kappa_1)(1 + \sigma_1) [-\hat{s}_1 + (1 - \beta_1)\hat{c}_1\hat{s}_1 + \beta_1\alpha_1\hat{c}_1], \\ \varepsilon_2 \frac{d\hat{c}_1}{dT} &= \hat{s}_1 - (1 - \beta_1)\hat{c}_1\hat{s}_1 - \beta_1\hat{c}_1, \end{aligned} \quad (37)$$

then the phase-plane trajectory should be  $\mathcal{O}(\varepsilon_2)$  from the  $c_1$ -nullcline when  $T = \varepsilon_2 \ln \varepsilon_2$ . Consequently, since  $T = t/t_{s_1}$ , we obtain

$$t = t_{s_1} \cdot \varepsilon_2 \ln \varepsilon_2 = t_{c_1} \ln \varepsilon_2 \approx t_{c_1}^* \quad (38)$$

as the asymptotic time required for  $c_1$  to reach its maximum value.

There is utility in computing  $t_{c_1}^*$ . Specifically, the timescale  $t_{c_1}^*$  allows us to partition the dynamics: for  $t < t_{c_1}^*$ , the dynamics are transient, and for  $t > t_{c_1}^*$  the dynamics are in the steady-state phase. However, it also indicates precisely *when* the rate of product formation reaches maximum steady-state production:

$$\max \dot{p} \simeq \dot{p}(t_{c_1}^*). \quad (39)$$

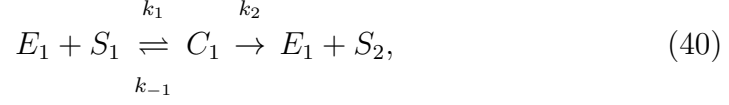
Thus, the matching timescale is a very good indication of how long it takes before the product formation rate reaches its maximum value, and when the reaction can be assumed to be in a steady-state phase.

#### 4. The auxiliary enzyme reaction mechanism

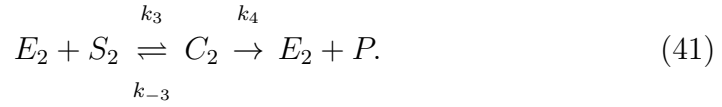
We now consider the more complicated case of the auxiliary enzyme reaction mechanism (Eilertsen and Schnell, 2018). The mechanism is composed



of two reactions: a primary reaction (40) that produces a substrate,  $S_2$ , that is synthesized in a catalytic step:



a secondary reaction, (41), where  $S_2$  binds with the auxiliary enzyme “ $E_2$ ” and releases the final product,  $P$ :



The complete set of mass action equations that model of the kinetics of the complete reaction mechanism are

$$\dot{s}_1 = -k_1(e_1^0 - c_1)s_1 + k_{-1}c_1, \quad (42a)$$

$$\dot{c}_1 = k_1(e_1^0 - c_1)s_1 - (k_{-1} + k_2)c_1, \quad (42b)$$

$$\dot{s}_2 = -k_3(e_2^0 - c_2)s_2 + k_{-3}c_2 + k_2c_1, \quad (42c)$$

$$\dot{c}_2 = k_3(e_2^0 - c_2)s_2 - (k_{-3} + k_4)c_2, \quad (42d)$$

where  $s_1$  and  $s_2$  denote the respective concentrations of the substrates  $S_1$  and  $S_2$ ,  $c_1$  and  $c_2$  denote the concentrations of the complexes  $C_1$  and  $C_2$ , and  $e_1^0$  and  $e_2^0$  denote the initial concentrations of the primary and auxiliary enzymes,  $E_1$  and  $E_2$ . We define the initial conditions for the secondary reaction as  $(s_2, c_2)(t = 0) = (0, 0)$ .

In forthcoming analysis, we will assume that the primary reaction is in its steady-state phase and it obeys RSA (i.e.,  $\varepsilon_1 \ll 1$ ). Additionally, we will make the assumption that  $k_2 \lesssim k_4$ , and that the initial auxiliary enzyme concentration is large (i.e.,  $e_2^0 \gg 1$ ).

#### 4.1. The study of phase-plane geometry of the auxiliary enzyme reaction mechanisms permit a heuristic estimation of characteristic timescales

Perhaps the most intuitive way to derive the relevant characteristic timescales of (40)–(41) is to get a qualitative understanding of what a typical phase-plane trajectory looks like in the  $c_2$ – $s_2$  plane. Numerical simulations suggest that the phase-plane trajectory is almost “triangular” in certain parameter ranges (see FIGURE 5) and, based on the appearance of the phase-plane trajectory (again, see FIGURE 5), there appears to be at least three distinct timescales:

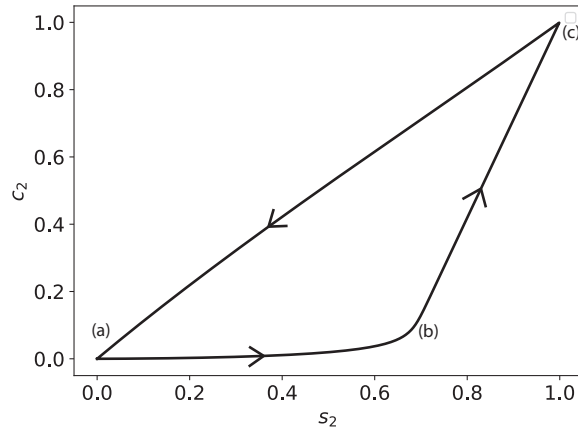


Figure 5: **The phase-plane portrait of the mass action trajectory for the auxiliary reaction mechanism (40)–(41).** The solid black curve is the numerically-computed solution to (42a)–(42d). The initial concentrations and rate constants used in the numerical simulation are:  $k_1 = 1$ ,  $k_2 = 1$ ,  $k_{-1} = 1$ ,  $e_1^0 = 1$ ,  $e_2^0 = 100$ ,  $k_{-3} = 1$ ,  $k_3 = 1$ ,  $k_4 = 2$  and  $s_1^0 = 100$  (units have been omitted).  $s_2$  and  $c_2$  have been scaled by their numerically-obtained maximum values.

- The scale on which the trajectory travels from (a) to (b). We will denote this timescale as  $t_{s_2}$ .
- The scale on which the trajectory travels from (b) to (c). We will denote this timescale as  $t_{c_2}$ .
- The scale on which the trajectory travels from (c) back to (a). We will denote this timescale as  $t_p$ .

The logical step that follows will be to make some initial *a priori* assumptions about the ordering of all the timescales involved in the reaction. For the sake of simplicity, let us initially assume that  $t_{c_1} \ll t_{s_2}, t_{c_2} \ll t_{s_1}$ , and that the *completion* timescale for the secondary reaction is identically  $t_{s_1}$ . This implies that the secondary reaction completes at roughly the same time as the primary reaction, and that  $t_p \approx t_{s_1}$ . Thus, we have eliminated one timescale ( $t_p$ ) by imposing the assumption that the secondary reaction is sufficiently fast.

The next step will be to exploit the presence and geometry of any manifolds (not necessarily invariant) that exist within the phase-plane of the secondary reaction. Notice that the intersection of the  $s_2$  and  $c_2$  nullclines is *time-dependent* since the  $s_2$ -nullcline moves as  $c_1$  varies in time. Geometrically, the intersection of the nullclines is described by a moving fixed point,  $\mathbf{x}^*$ ,

$$N_{s_2} \cap N_{c_2} \equiv \mathbf{x}^*, \quad (43)$$

where  $N_{s_2}$  denotes the  $s_2$ -nullcline and  $N_{c_2}$  denotes the  $c_2$ -nullcline. Algebraically, the coordinates of  $\mathbf{x}^*$ ,  $(s_2^*, c_2^*)$ , are

$$s_2^* = \frac{K_{M_2} k_2 c_1(t)}{V_2 - k_2 c_1(t)}, \quad c_2^* = \frac{k_2 c_1(t)}{k_4}, \quad (44)$$

where  $K_{M_2}$  denotes the Michaelis constant of the secondary reaction

$$K_{M_2} \equiv \frac{k_{-3} + k_4}{k_3}, \quad (45)$$

and  $V_2$  denotes the limiting rate of the secondary reaction:  $V_2 \equiv e_2^0 k_4$ .

Since the position of  $s_2$ -nullcline depends on the concentration  $c_1$ , we want to estimate how  $c_1$  varies over the course of the reaction. As we are assuming that the primary reaction follows the RSA, the phase plane trajectory will follow a slow manifold when  $t \geq t_{c_1}^*$ . If we know the shape of the slow manifold, then we can get a rough idea of how  $c_1$  varies throughout the reaction. To do this, we will look at the dimensionless equations

$$\begin{aligned} \frac{d\hat{s}_1}{dT} &= (1 + \kappa_1)(1 + \sigma_1) [-\hat{s}_1 + (1 - \beta_1)\hat{c}_1\hat{s}_1 + \beta_1\alpha_1\hat{c}_1], \\ \varepsilon_2 \frac{d\hat{c}_1}{dT} &= \hat{s}_1 - (1 - \beta_1)\hat{c}_1\hat{s}_1 - \beta_1\hat{c}_1. \end{aligned} \quad (46)$$

The zeroth order asymptotic approximation to the slow manifold is the  $\hat{c}_1$ -nullcline:

$$\hat{s}_1 - (1 - \beta_1)\hat{c}_1\hat{s}_1 - \beta_1\hat{c}_1 = 0. \quad (47)$$

Notice that  $\beta_1 \rightarrow 0$  as  $\sigma_1 \rightarrow \infty$ , and thus, as  $\sigma_1 \rightarrow \infty$ , the trajectory that follows the slow manifold will be asymptotic to the curve  $\hat{c}_1 = 1$  for most of the reaction. Hence, when  $\sigma_1 \gg 1$ , the concentration of the intermediate complex remains near its maximum value,  $c_1^{\max}$ , for the majority of the reaction, and

the  $s_2$ -nullcline will be effectively stationary after the initial buildup of  $c_1$ . This suggests that, under the assumption that  $t_{c_1}$  is the shortest timescale, the initial transient behavior of  $c_2$  will occur while the  $s_2$ -nullcline remains fixed; thus, we look at the phase-plane trajectory with the  $s_2$ -nullcline (with fixed  $c_1$ ) at its stationary value (see FIGURE 6). Let us denote this manifold as  $N_{s_2}^{\max}$ :

$$N_{s_2}^{\max} \equiv \left\{ (s_2, c_2) \in \mathbb{R}^2 : c_2 - \frac{k_3 e_2^0 s_2 - k_2 c_1^{\max}}{k_3 s_2 + k_{-3}} = 0 \right\}. \quad (48)$$

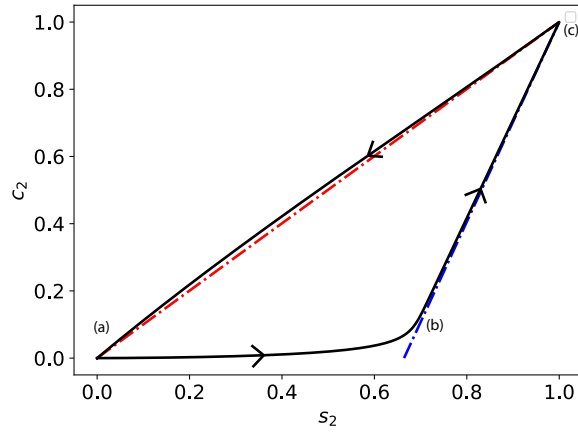


Figure 6: **The  $s_2$ - $c_2$  phase-plane trajectory (with nullclines) for the auxiliary reaction mechanism (40)–(41).** The thick black curve is the numerically-integrated solutions to the mass action equations (42a)–(42d). The broken red curve is the  $c_2$ -nullcline, and the broken blue curve is the fixed  $s_2$ -nullcline,  $N_{s_2}^{\max}$ . The phase-plane trajectory initially moves towards  $N_{s_2}^{\max}$ , then moves up  $N_{s_2}^{\max}$  before moving back down the  $c_2$ -nullcline. The constants (without units) used in the numerical simulation are:  $e_1^0 = 1$ ,  $s_1^0 = 100$ ,  $k_1 = 1$ ,  $k_2 = 1$ ,  $k_3 = 1$ ,  $k_{-3} = 1$ ,  $k_4 = 2$ ,  $e_2^0 = 100$  and  $k_{-1} = 1$ .

We will first estimate  $t_{s_2}$  by noting that the phase-plane trajectory essentially lies along the  $s_2$ -axis for  $t \leq t_{s_2}$ . This suggests that

$$\dot{s}_2 \approx -k_3 s_2 + k_2 c_1, \quad t \leq t_{s_2} \quad (49)$$

is a reasonable approximation to (42c). If the initial fast transient of the primary reaction is negligibly short, i.e.,  $t_{c_1} \ll t_{s_2}$ , then it is reasonable to assume

$$\dot{s}_2 \approx -k_3 s_2 + k_2 c_1^{\max}, \quad t \leq t_{s_2}. \quad (50)$$

Since (50) is linear, its exact solution,

$$s_2 \approx s_2^\lambda [1 - \exp(-t/t_{s_2})], \quad (51)$$

provides two critical estimates: the characteristic timescale,  $t_{s_2}$ , and an approximate maximum value of  $s_2$  on the  $t_{s_2}$  timescale:

$$t_{s_2} \equiv \frac{1}{k_3 e_2^0}, \quad s_2 \leq s_2^\lambda \equiv \frac{k_2 c_1^{\max}}{k_3 e_2^0}. \quad (52)$$

The prediction that  $s_2 < s_2^{\max}$  for  $t \leq t_{s_2}$  (obtained from the linear equation) is in qualitative agreement with the phase-plane trajectory of the numerically-integrated equations (FIGURE 6).

Next, to estimate  $t_{c_2}$ , we note that since the phase-plane trajectory lies close to  $N_{s_2}^{\max}$  along its ascension to  $c_2^{\max}$ , the growth of the intermediate complex is approximately

$$\dot{c}_2 \approx -k_4 c_2 + k_2 c_1^{\max}, \quad t_{s_2} \leq t \leq t_{c_2}, \quad (53)$$

which admits an analytical solution:

$$c_2 \approx c_2^{\max} [1 - \exp(-k_4 t)]. \quad (54)$$

Trajectories that follow the  $s_2$ -nullcline closely are said to be in a reverse quasi-steady-state (Schnell and Maini, 2000) or rapid equilibrium (Rousset and Fraser, 1991); this is in contrast to trajectories that follow the  $c_2$ -nullcline, which are said to be in a steady-state phase (Eilertsen and Schnell, 2018). From (54) we have two observations: (i)  $k_4^{-1}$  is a reasonable estimate of  $t_{c_2}$ , and (ii), the linearized solution predicts  $c_2$  will approach  $c_2^{\max}$ , which is in qualitative agreement with the phase-plane trajectory.

#### 4.2. Scaling analysis: Designation of slow and fast timescales

Although we now have estimates for the timescales  $t_{s_2}$  and  $t_{c_2}$ , it is important to remember that these timescales were obtained under the assumption that  $c_1$  is the fastest variable (i.e.,  $c_1$  reaches its maximum before any other variable). If the second reaction is sufficiently fast, then the phase-plane geometry suggests that the trajectory should not only catch the fixed point  $\mathbf{x}^*$ , but will also *adhere* to  $\mathbf{x}^*$  as it descends to the origin. If the trajectory

can adhere to  $\mathbf{x}^*$ , then

$$\dot{p} = \frac{V_2 \frac{K_{M_2} k_2 c_1}{V_2 - k_2 c_1}}{K_{M_2} + \frac{K_{M_2} k_2 c_1}{V_2 - k_2 c_1}} = k_2 c_1, \quad (55)$$

and the product formation rate of the secondary reaction has reached its limiting value. We must now: (i) determine the appropriate conditions under which adhesion is possible, and (ii) determine the onset of validity for (55). We begin by scaling the mass action equations. Introducing the additional scaled concentrations

$$\hat{s}_2 = s_2/s_2^{\max}, \quad \hat{c}_2 = c_2/c_2^{\max}, \quad (56)$$

into equations (42c)–(42d) admits the dimensionless form:

$$\mu_1 \frac{d\hat{s}_2}{dT} = \left[ \left( \frac{\sigma_2}{1 + \sigma_2} \hat{c}_2 - 1 \right) \hat{s}_2 + \frac{\kappa_2}{(1 + \sigma_2)(1 + \kappa_2)} \hat{c}_2 \right] + \delta \mu_1 \hat{c}_1, \quad (57a)$$

$$\mu_2 \frac{d\hat{c}_2}{dT} = (1 + \kappa_2)(1 + \sigma_2) \left[ \left( 1 - \frac{\sigma_2}{1 + \sigma_2} \hat{c}_2 \right) \hat{s}_2 - \frac{1}{1 + \sigma_2} \hat{c}_2 \right]. \quad (57b)$$

The dimensionless parameters  $\kappa_2$ ,  $\sigma_2$ , and  $\delta$ , introduced in (57a)–(57b), are

$$\kappa_2 \equiv \frac{k_{-3}}{k_4}, \quad \sigma_2 \equiv \frac{s_2^{\max}}{K_{M_2}}, \quad \delta \equiv \frac{s_1^0}{s_2^{\max}}. \quad (58)$$

The remaining parameters,  $\mu_1$  and  $\mu_2$ , are the ratios of the accumulation timescales to the depletion timescale:

$$\mu_1 \equiv \frac{t_{s_2}}{t_{s_1}}, \quad \mu_2 \equiv \frac{t_{c_2}}{t_{s_1}}. \quad (59)$$

It follows from (59) that if  $\{\varepsilon_1, \mu_1, \mu_2\} \ll 1$ , then the dynamics of (42a)–(42d) consist of one slow variable,  $s_1$ , and three fast variables:  $c_1$ ,  $s_2$  and  $c_2$ . The designation of  $s_1$  as a slow variable and  $c_1$ ,  $s_2$  and  $c_2$  as fast variables implies that after an initial fast transient, the phase-plane trajectory is asymptotic

to the intersecting nullclines:

$$s_2 \simeq \frac{K_{M_1}}{V_2 - k_2 c_1} k_2 c_1, \quad (60a)$$

$$c_2 \simeq \frac{k_2 c_1}{k_4}. \quad (60b)$$

Additionally, after the initial fast transient of the primary reaction,  $k_2 c_1$  is asymptotic to

$$k_2 c_1 \simeq \frac{V_1}{K_{M_1} + s_1} s_1 \equiv -\dot{s}_1^\varepsilon, \quad (61)$$

and thus  $c_1$ ,  $s_2$  and  $c_2$  are, in the asymptotic limit, explicitly dependent on  $s_1$  only:

$$s_2 \simeq -\frac{K_{M_1}}{V_2 + \dot{s}_1^\varepsilon} \dot{s}_1^\varepsilon, \quad (62a)$$

$$c_2 \simeq -\frac{1}{k_4} \dot{s}_1^\varepsilon. \quad (62b)$$

The question that remains to be addressed is: ‘‘How much time must elapse (i.e., the lag time) before (62a)–(62b) are applicable?’’ To answer this question, we rescale (42c)–(42d) with respect to  $\tau = t/t_{c_1}$ :

$$\lambda_1 \frac{d\hat{s}_2}{d\tau} = \left[ \left( \frac{\sigma_2}{1 + \sigma_2} \hat{c}_2 - 1 \right) \hat{s}_2 + \frac{\kappa_2}{(1 + \sigma_2)(1 + \kappa_2)} \hat{c}_2 \right] + \delta\mu_1 \hat{c}_1, \quad (63a)$$

$$\lambda_2 \frac{d\hat{c}_2}{d\tau} = (1 + \kappa_2)(1 + \sigma_2) \left[ \left( 1 - \frac{\sigma_2}{1 + \sigma_2} \hat{c}_2 \right) \hat{s}_2 - \frac{1}{1 + \sigma_2} \hat{c}_2 \right]. \quad (63b)$$

The parameters that emerge from scaling,  $\lambda_1$  and  $\lambda_2$ , are the ratios we need in order to calculate the lag time that occurs before (62a)–(62b) become valid approximations:

$$\lambda_1 = \frac{t_{s_2}}{t_{c_1}}, \quad \lambda_2 = \frac{t_{c_2}}{t_{c_1}}. \quad (64)$$

From (63a)–(63b) it is clear that if  $t_{c_1} \ll t_{s_2}$ , then

$$s_2 < k_2 c_1^{\max} \cdot t_{c_1} \ll s_2^\lambda, \quad (65)$$

and  $s_2$  is a slow variable with respect to the  $t_{c_1}$  timescale. Thus, if  $t_{c_1} \ll t_{s_2} + t_{c_2}$ , then the lag time is roughly

$$t_{c_1} + t_{s_2} + t_{c_2} \approx t_{s_2} + t_{c_2} \equiv T_L. \quad (66)$$

As a result of the particular ordering of the timescales, the auxiliary reaction

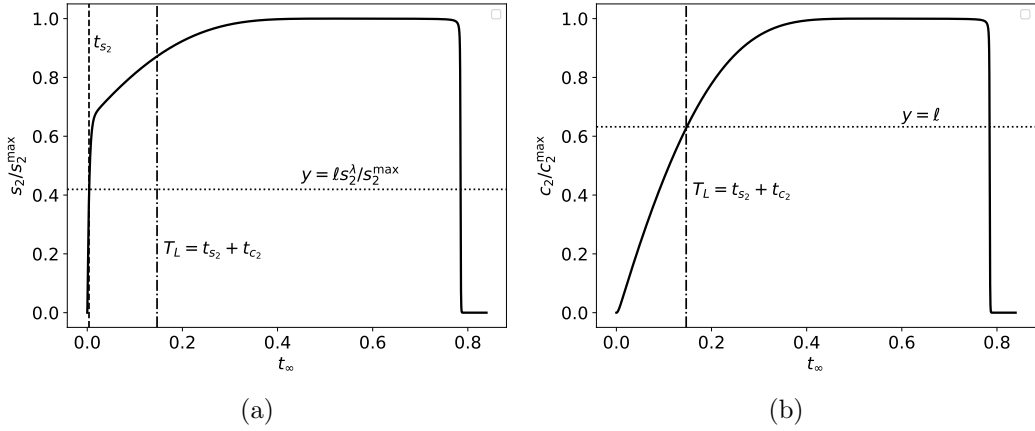


Figure 7: **The timescales  $t_{s_2}$  and  $T_L$  are characteristic of the time it takes  $s_2$  to reach  $s_2^\lambda$  and  $c_2$  to reach  $c_2^{\max}$ , respectively, in the auxiliary reaction mechanism (40)–(41).** The thick black curves are the numerically-integrated solutions to the mass action equations (42a)–(42d). The dashed/dotted vertical lines correspond to  $T_L$ , and the dashed vertical line (Panel (a)) corresponds to  $t_{s_2}$ . In Panel (a), the dotted horizontal line corresponds to the scaled characteristic value  $\ell s_2^\lambda$ . In Panel (b), the dotted horizontal line corresponds to the scaled characteristic value  $\ell c_2^{\max}$ . Notice that when  $t_{c_1} \ll t_{s_2} + t_{c_2}$ , the timescale  $t_{s_2}$  is characteristic of the time it takes for  $s_2$  to reach  $s_2^\lambda$  (Panel (a)), and  $T_L$  is characteristic of the time it takes  $c_2$  to reach  $c_2^{\max}$  (Panel (b)). The constants (without units) used in the numerical simulation are:  $e_1^0 = 1$ ,  $s_1^0 = 100$ ,  $e_2^0 = 100$ ,  $k_1 = 10$ ,  $k_2 = 1$ ,  $k_3 = 1$ ,  $k_{-3} = 1$ ,  $k_4 = 2$  and  $k_{-1} = 1$ . Time has been mapped to the  $t_\infty$  scale:  $t_\infty(t) = 1 - 1/\ln(t + e)$ , and the values of  $s_2$  and  $c_2$  have been numerically-scaled by their maximum values.

mechanisms dynamics can be partitioned into an initial layer (67a), an inner



layer (67b), and an outer layer (67c):

$$\begin{cases} c_2 \simeq 0, \\ s_2 \simeq s_2^\lambda [1 - \exp(-t/t_{s_2})], \end{cases} \quad t \lesssim t_{s_2} \quad (67a)$$

$$\begin{cases} c_2 \simeq c_2^{\max} [1 - \exp(-t/t_{c_2})], \\ s_2 \simeq \frac{k_{-3}c_2 + k_2c_1^{\max}}{k_3(e_2^0 - c_2)}, \end{cases} \quad t_{s_2} \lesssim t \lesssim T_L \quad (67b)$$

$$\begin{cases} s_2 \simeq -\frac{K_{M_2}}{V_2 + \dot{s}_1^\varepsilon} \dot{s}_1^\varepsilon, \\ c_2 \simeq \frac{e_2^0}{K_{M_2} + s_2} s_2. \end{cases} \quad T_L \lesssim t \quad (67c)$$

Furthermore, the characteristic timescales allow us to formally construct the composite solutions for  $s_2$  and  $c_2$

$$s_2^{io} = -s_2^\lambda [\exp(-t/t_{s_2})] + \frac{k_{-3}c_2^{io} + k_2c_1^{\max}}{k_3(e_2^0 - c_2^{io})} - \frac{K_{M_2}}{V_2 + \dot{s}_1^\varepsilon} \dot{s}_1^\varepsilon - s_2^{\max}, \quad (68a)$$

$$c_2^{io} = -c_2^{\max} [\exp(-t/t_{c_2})] - \dot{s}_1^\varepsilon/k_4, \quad (68b)$$

which are constructed from the piecewise descriptions of the kinetics with respect to each timescale: they provide a uniform asymptotic expansion that is valid for all time (FIGURES 8a–8b).

#### 4.3. Multiple layers and multiple matching timescales

In the previous section, we derived inner (initial fast transient) and outer (steady-state phase) solutions. Specifically, we found that if  $t_{c_1} \ll t_{c_2}, t_{s_2} \ll t_{s_1}$ , then the solution can be approximated with an initial layer (67a), an inner layer (67b), and an outer layer (67c). Now, let  $t_{s_2}^*$  denote the actual time it takes  $s_2$  to reach  $s_2^*$ , and let  $T_L^*$  denote the actual time it takes  $s_2$  and  $c_2$  to reach  $\boldsymbol{x}^*$ . Since  $t_{s_2}$  and  $T_L$  are characteristic timescales, utilizing them as *matching* timescales is problematic since the transition regimes,

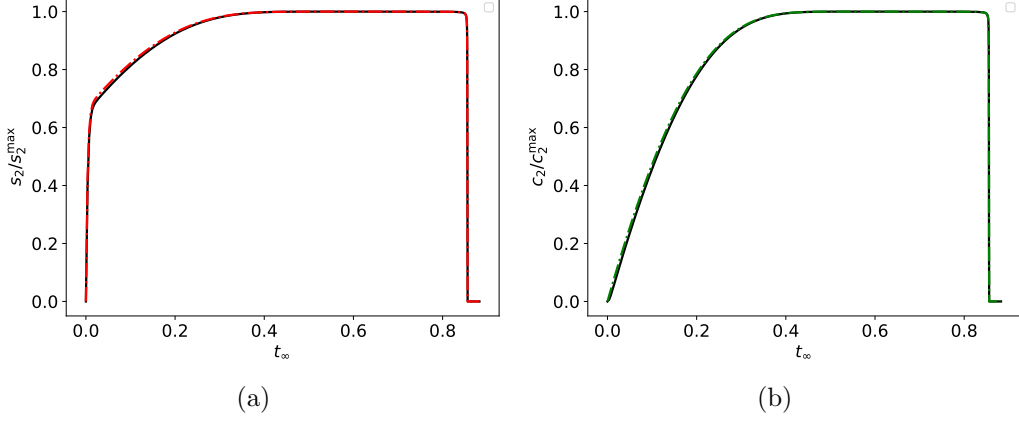


Figure 8: **A graphical illustration of the accuracy of the composite solutions for the auxiliary reaction mechanism (40)–(41).** Panel (a): The solid black curve (barely visible) is the numerical solution to (42c), and the dash/dotted red curve is the composite solution (68a). Panel (b): The solid black curve (again, barely visible) is the numerical solution to (42d), and the dashed/dotted green curve is the composite solution (68b). The constants (without units) used in the numerical simulation are:  $e_1^0 = 1$ ,  $s_1^0 = 1000$ ,  $e_2^0 = 100$ ,  $k_1 = 1$ ,  $k_2 = 1$ ,  $k_3 = 1$ ,  $k_{-3} = 1$ ,  $k_4 = 2$  and  $k_{-1} = 1$ . Time has been mapped to the  $t_\infty$  scale:  $t_\infty(t) = 1 - 1/\ln(t + e)$ . Concentrations have been scaled by their maximum values.

$t_{s_2} \leq t \leq t_{s_2}^*$  and  $T_L \leq t \leq T_L^*$ , can be quite large. Thus, what we really want are reliable estimates for  $t_{s_2}^*$  and  $T_L^*$ . To construct these estimates, we will utilize the approximation techniques introduced in Section 3. Starting with  $t_{s_2}^*$ , we observe that if  $c_2 \simeq 0$  for  $t \lesssim t_{s_2}$ , then it is necessary that  $c_2$  scale as a slow variable with respect to  $t_{s_2}$ . Rescaling (42d) with respect to  $\bar{T} = t/t_{s_2}$  yields

$$\frac{d\hat{s}_2}{d\bar{T}} = \left( \frac{\sigma_2}{1 + \sigma_2} \hat{c}_2 - 1 \right) \hat{s}_2 + \frac{1}{1 + \sigma_2} \hat{c}_2 + \delta\mu_1 \hat{c}_1 \quad (69a)$$

$$\frac{d\hat{c}_2}{d\bar{T}} = \nu(1 + \kappa_2)(1 + \sigma_2) \left[ \left( 1 - \frac{\sigma_2}{1 + \sigma_2} \hat{c}_2 \right) \hat{s}_2 - \frac{1}{1 + \sigma_2} \hat{c}_2 \right], \quad (69b)$$

where  $\nu \equiv t_{s_2}/t_{c_2}$ . Thus, it is clear from (69b) that if  $\nu(1 + \kappa_2)(1 + \sigma_2) \ll 1$ , then  $c_2 \simeq 0$  for  $t \lesssim t_{s_2}$ , and

$$t_{s_2}^* \approx -t_{s_2} \ln t_{s_2}/t_{c_2}, \quad (70)$$

is a reliable approximation for  $t_{s_2}^*$  provided  $t_{c_1} \ll t_{s_2} \ll t_{c_2} \ll t_{s_1}$ .

To determine an appropriate approximation for  $T_L^*$ , we rescale (13a) and (42d) with respect to  $T = t/t_{s_1}$ :

$$\frac{d\hat{s}_1}{dT} = \omega(1 + \kappa_1)(1 + \sigma_1) [-\hat{s}_1 + (1 - \beta_1)\hat{c}_1\hat{s}_1 + \beta_1\alpha_1\hat{c}_1], \quad (71a)$$

$$\mu_2 \frac{d\hat{c}_2}{dT} = (1 + \kappa_2)(1 + \sigma_2) \left[ \left(1 - \frac{\sigma_2}{1 + \sigma_2}\hat{c}_2\right)\hat{s}_2 - \frac{1}{1 + \sigma_2}\hat{c}_2 \right]. \quad (71b)$$

We have ignored equations (13b) and (42c) since their dynamics are determined to first order by slow manifolds. Thus, it follows from Theorem 1 that

$$T_L^* \approx -t_{c_2} \ln \mu_2, \quad (72)$$

which again will hold provided  $t_{c_1} \ll t_{s_2} \ll t_{c_2} \ll t_{s_1}$ . Consequently, the approximated matching timescales,  $t_{s_2}^*$  and  $T_L^*$ , allow us to construct a more *precise* partition of the various regimes (see FIGURES 9a–9c):

$$\begin{cases} c_2 \simeq 0, \\ s_2 \simeq s_2^\lambda [1 - \exp(-t/t_{s_2})], \end{cases} \quad t \leq t_{s_2}^* \quad (73a)$$

$$\begin{cases} c_2 \simeq c_2^{\max} [1 - \exp(-t/t_{c_2})], \\ s_2 \simeq \frac{k_{-3}c_2 + k_2c_1^{\max}}{k_3(e_2^0 - c_2)}, \end{cases} \quad t_{s_2}^* \leq t \leq T_L^* \quad (73b)$$

$$\begin{cases} s_2 \simeq -\frac{K_{M_2}}{V_2 + \dot{s}_1^\varepsilon} \dot{s}_1^\varepsilon, \\ c_2 \simeq \frac{e_2^0}{K_{M_2} + s_2} s_2. \end{cases} \quad T_L^* \leq t \quad (73c)$$

From (73a)–(73c) we see that the lag time (i.e., the time it takes the trajectory to reach  $\mathbf{x}^*$ ), specific to the ordering  $t_{c_1} \ll t_{s_2} \ll t_{c_2} \ll t_{s_1}$ , is approximately  $T_L^*$  and the product formation rate beyond the lag time is

$$\dot{p} \simeq \frac{V_1}{K_{M_1} + s_1} s_1, \quad t \geq T_L^*. \quad (74)$$

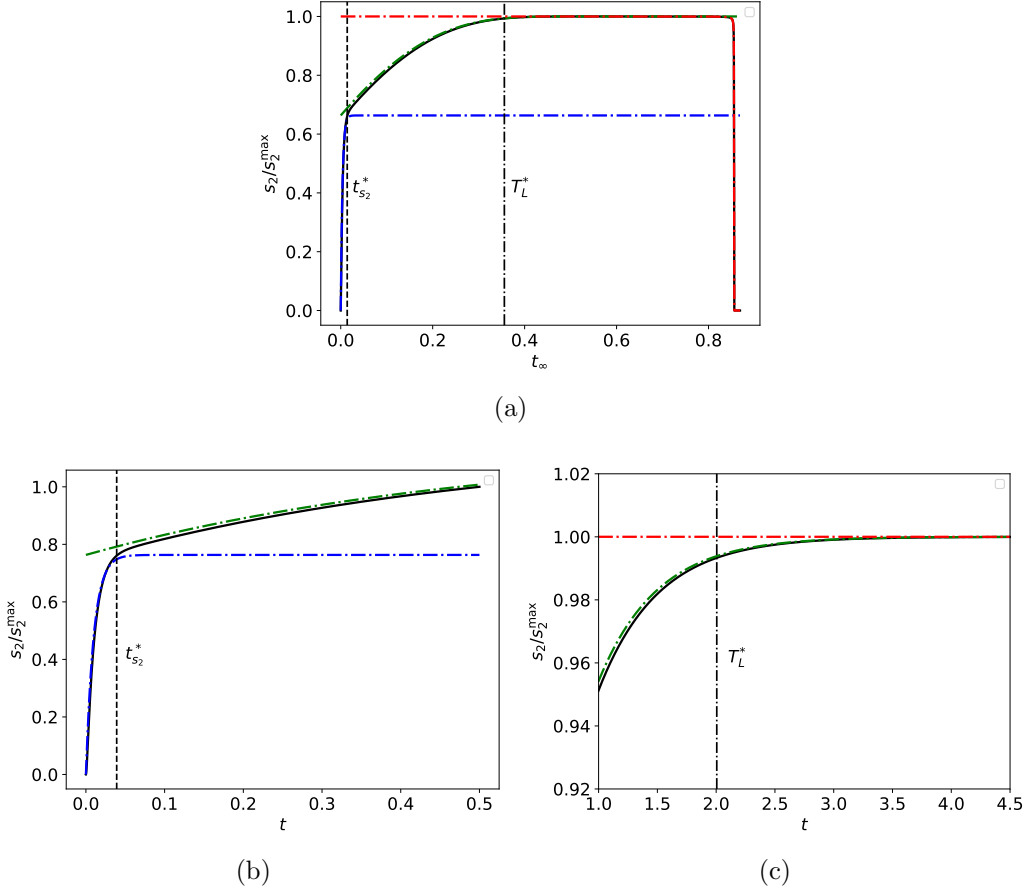


Figure 9: **The graphical visualization and validity of the matching timescales for the auxiliary reaction mechanism (40)–(41).** Panel (a): The solid black curve is the numerical solution to (42c), the dashed/dotted blue curve is the initial solution (67a), the dashed/dotted green curve is the inner solution (67b) and the dash/dotted red curve is the outer solution (67c). Time has been mapped to the  $t_\infty$  timescale in panel (a). Panels (b) and (c) are close-ups of panel (a) near the transition regions. Panel (b) is the transition near  $t_{s_2}^*$  and Panel (c) is the transition near  $T_L^*$ . The constants (without units) used in the numerical simulation are:  $e_1^0 = 1$ ,  $s_1^0 = 1000$ ,  $e_2^0 = 100$ ,  $k_1 = 1$ ,  $k_2 = 1$ ,  $k_3 = 1$ ,  $k_{-3} = 1$ ,  $k_4 = 2$  and  $k_{-1} = 1$ . Time is unmapped in panels (b) and (c).

#### 4.4. Alternative orderings of timescales for the auxiliary reaction mechanism

The results obtained in the previous subsection we derived under the condition that  $t_{c_1} \ll t_{s_2} \ll t_{c_2} \ll t_{s_1}$ . There are two additional orderings that can be analyzed for fast secondary reactions:  $t_{c_1} \ll t_{c_2} \ll t_{s_2} \ll t_{s_1}$ , and  $\{t_{c_2}, t_{s_2}\} \ll t_{c_1} \ll t_{s_1}$ . The former of these orderings,  $t_{c_1} \ll t_{c_2} \ll t_{s_2} \ll t_{s_1}$ ,

provides a condition for the quasi-steady-state assumption to hold for roughly the duration of the secondary reaction. To see why, we first note that if  $t_{c_2} \ll t_{s_2}$ , then  $\nu(1 + \sigma_2)(1 + \kappa_2) \gg 1$ . Consequently, since

$$(1 + \sigma_2)(1 + \kappa_2)\nu = \frac{K_{M_2} + s_2^{\max}}{e_2^0}, \quad (75)$$

equations (69a)–(69b) can be expressed as

$$\frac{d\hat{s}_2}{dT} = \left( \frac{\sigma_2}{1 + \sigma_2} \hat{c}_2 - 1 \right) \hat{s}_2 + \frac{1}{1 + \sigma_2} \hat{c}_2 + \delta\mu_1 \hat{c}_1, \quad (76a)$$

$$\lambda^* \frac{d\hat{c}_2}{dT} = \left( 1 - \frac{\sigma_2}{1 + \sigma_2} \hat{c}_2 \right) \hat{s}_2 - \frac{1}{1 + \sigma_2} \hat{c}_2, \quad (76b)$$

If  $\lambda^*$  is small, then the trajectory will tend to crawl up the  $c_2$ -nullcline towards  $\mathbf{x}^*$ . However, in this case,  $t_{s_2}$  is *not* the characteristic time it takes for the trajectory to reach  $\mathbf{x}^*$ . We will not go into the details of the scenario here, since the results can be found in (Eilertsen and Schnell, 2018).

On the other hand, if the ordering  $\{t_{s_2}, t_{c_2}\} \ll t_{c_1} \ll t_{s_1}$  is observed, then the asymptotic solution consists of *two* layers

$$\begin{cases} s_2 \simeq \frac{K_{M_2}}{V_2 - k_2 c_1^\varepsilon} k_2 c_1^\varepsilon, \\ c_2 \simeq \frac{e_2^0}{K_{M_2} + s_2} s_2, \end{cases} \quad t \leq t_{c_1}^* \quad (77a)$$

$$\begin{cases} s_2 \simeq -\frac{K_{M_2}}{V_2 + \hat{s}_1^\varepsilon} \hat{s}_1^\varepsilon, \\ c_2 \simeq \frac{e_2^0}{K_{M_2} + s_2} s_2, \end{cases} \quad t_{c_1}^* \leq t \quad (77b)$$

and the lag time is approximately  $t_{c_1}^*$  (see FIGURES 10a and 10b). The accuracy of  $t_{c_1}^*$  as a lag time for the ordering  $\{t_{s_2}, t_{c_2}\} \ll t_{c_1} \ll t_{s_1}$  follows from the fact that  $t_{c_1}$  is a characteristic timescale when  $c_2$  and  $s_2$  are roughly as fast as  $c_1$  (see FIGURES 11a and 11b). Thus, the natural lag time is given by  $t_{c_1}^*$  when  $s_2$  and  $c_2$  are nearly as fast as  $c_1$ .

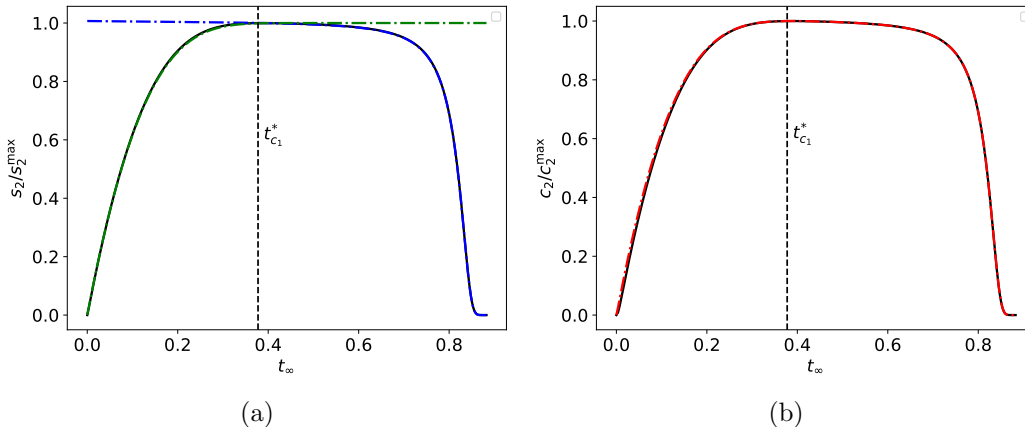


Figure 10: **The timescale  $t_{c_1}^*$  is a valid matching timescale for extremely fast secondary reactions in the auxiliary reaction mechanism (40)–(41).** The thick black curves (barely visible) are the numerically-integrated solutions to the mass action equations (42a)–(42d). The dashed vertical lines correspond to  $t_{c_1}^*$ . In Panel (a), the dashed/dotted green line corresponds to the inner solution (77a), and the dashed/dotted blue line corresponds to the outer solution (77b). In Panel (b), the dashed/dotted red curve corresponds to the QSS solution (77a)–(77b). The constants (without units) used in the numerical simulation are:  $e_1^0 = 1$ ,  $s_1^0 = 100$ ,  $e_2^0 = 1000$ ,  $k_1 = 0.01$ ,  $k_2 = 1$ ,  $k_3 = 1$ ,  $k_{-3} = 1$ ,  $k_4 = 100$  and  $k_{-1} = 1$ . Time has been mapped to the  $t_\infty$  scale:  $t_\infty(t) = 1 - 1/\ln(t + e)$ , and the values of  $s_2$  and  $c_2$ , as well as the asymptotic solutions (77a)–(77b), have been scaled by their numerically-computed maximum values.

## 5. Discussion

Enzyme catalyzed reactions typically consist of multiple regimes; each regime marks a domain over which certain kinetic behavior and corresponding rate laws can be assumed to be valid. The primary contribution of this paper was to categorize specific types of timescales, particularly with regard to matched asymptotics in enzyme catalyzed reactions. In short, we have shown that in each kinetic regime of a reaction there really exist two distinct timescales that must be considered: characteristic and matching. The characteristic timescale is an *accurate* timescale, and provides a rough estimate of the duration of a particular regime. As such, the characteristic timescale should be utilized in scaling analysis, as well as in the construction of the composite solution, since it determines the relevant length scale of its corresponding regime. However, its limitation resides in the fact that it is accurate but not *precise*. The matching timescale is precise, and determines

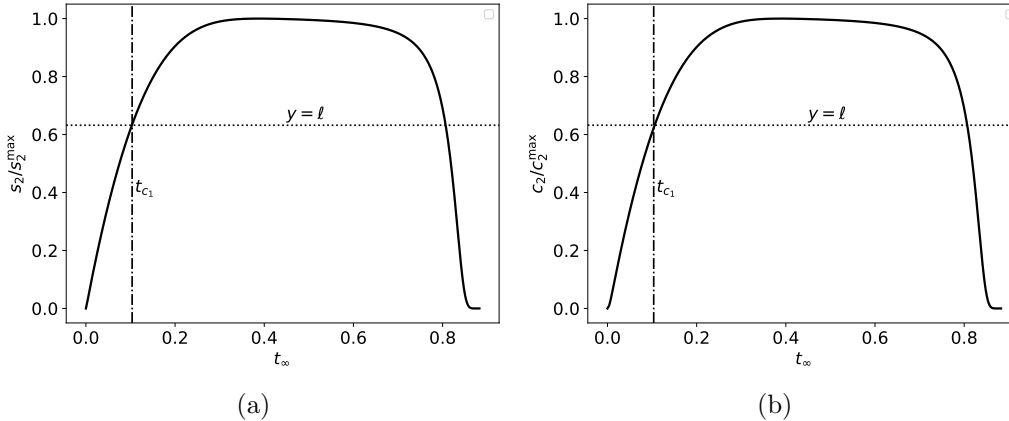


Figure 11: **The timescale  $t_{c_1}$  is a characteristic timescale of the secondary reaction when it is extremely fast in the auxiliary reaction mechanism (40)–(41).** The thick black curves are the numerically-integrated solutions to the mass action equations (42a)–(42d). The dashed/dotted vertical lines correspond to  $t_{c_1}$ . In Panel (a), the dotted horizontal line corresponds to the scaled characteristic value  $\ell s_2^{\max}$ . In Panel (b), the dotted horizontal line corresponds to the scaled characteristic value  $\ell c_2^{\max}$ . Notice that  $t_{c_1}$  is characteristic of the time it takes for both  $s_2$  and  $c_2$  to reach their threshold values. The constants (without units) used in the numerical simulation are:  $e_1^0 = 1$ ,  $s_1^0 = 100$ ,  $e_2^0 = 1000$ ,  $k_1 = 0.01$ ,  $k_2 = 1$ ,  $k_3 = 1$ ,  $k_{-3} = 1$ ,  $k_4 = 100$  and  $k_{-1} = 1$ . Time has been mapped to the  $t_\infty$  scale:  $t_\infty(t) = 1 - 1/\ln(t + e)$ , and the values of  $s_2$  and  $c_2$  have been numerically-scaled by their maximum values.

the temporal boundary of the corresponding regime.

In this work, the fast and slow timescales of the single-enzyme, single-substrate MM reaction mechanism (12) have been revisited. Under the RSA, the established fast timescale,  $t_{c_1}$ , of the MM reaction mechanism is a characteristic timescale: it provides the temporal order of magnitude needed for the concentration of complex to accumulate to approximately 63% of its threshold value. Again, it is *the* correct timescale from which to conduct scaling analysis. However, since  $t_{c_1}$  does not precisely determine when the complex concentration reaches its maximum value, it fails to define an appropriate matching timescale. The matching timescale delimits the precise time point in the course of the reaction when the transition from initial fast transient to steady-state kinetics occurs. By utilizing Tikhonov/Fenichel theory, we have shown that the appropriate matching timescale for the MM reaction

mechanism is  $t_{c_1}^*$ :

$$t_{c_1}^* = -t_{c_1} \ln \frac{t_{c_1}}{t_{s_1}}.$$

In addition, the auxiliary enzyme reaction mechanism (40)–(41) was analyzed with the assumption that the auxiliary enzyme concentration is high, and that the primary reaction obeys the RSA. We demonstrated that when the secondary reaction has sufficient speed, the overall kinetics and reaction mechanism is determined by the ratios of four *characteristic* timescales:  $t_{c_1}$ ,  $t_{s_2}$ ,  $t_{c_2}$  and  $t_{s_1}$ . Three different orderings of these timescales were considered: (i)  $t_{c_1} \ll t_{s_2} \ll t_{c_2} \ll t_{s_1}$ , (ii)  $t_{c_1} \ll t_{c_2} \ll t_{s_2} \ll t_{s_1}$ , and (iii)  $\{t_{c_2}, t_{s_2}\} \ll t_{c_1} \ll t_{s_1}$ . Specifically, with respect to the first ordering, (i), it was shown that the secondary reaction consisted of three layers: an initial fast transient, a secondary *inner* reverse-quasi-steady-state layer, and an outer, quasi-steady-state layer. For each layer an appropriate matching timescale was calculated that clearly and precisely establishes the boundary of the corresponding layer (regime). A composite solution, valid for the entire time course of the reaction, was also calculated; the asymptotic accuracy of the composite solution (with respect to ordering (i)) is essentially dependent on three timescale ratios:

$$\frac{t_{c_1}}{t_{s_2}} \ll 1, \quad \frac{t_{s_2}}{t_{c_2}} \ll 1, \quad \frac{t_{c_2} + t_{s_2}}{t_{s_1}} \ll 1.$$

The subtle difference between characteristic and matching timescales is often neglected in applications of GSPT. This work provides a useful case study in the rigorous interpretation of timescales in enzyme-catalyzed reactions, and the approaches used should be readily applicable to a wide range of singular perturbation problems in mathematical biology.

## Acknowledgements

This work is partially supported by the University of Michigan Protein Folding Diseases Initiative, and Beilstein-Institut zur Förderung der Chemischen Wissenschaften through its Beilstein Enzymology Symposia. We are grateful to Antonio Baici (University of Zurich) for helpful discussions about this work during the 2017 Beilstein Enzymology Symposia (Rüdesheim, Germany). WS is a fellow of the Michigan IRACDA program (NIH/NIGMS grant: K12 GM111725).



## References

- Berglund, N., Gentz, B., 2006. Noise-induced phenomena in slow-fast dynamical systems. Springer-Verlag London, Ltd., London.
- Bertram, R., Rubin, J. E., 2017. Multi-timescale systems and fast-slow analysis. *Math. Biosci.* 287, 105–121.
- Burke, M., Maini, P., Murray, J., 1993. Suicide substrate reaction-diffusion equations: Varying the source. *Mathematical Medicine and Biology* 10, 97–114.
- Burke, M. A., Maini, P., Murray, J., 1990. On the kinetics of suicide substrates. *Biophys. Chem.* 37, 81–90.
- Clark, A. R., Stokes, Y. M., Thompson, J. G., 2011. Estimation of glucose uptake by ovarian follicular cells. *Ann. Biomed. Eng.* 39, 2654–2667.
- Eilertsen, J., Schnell, S., 2018. A kinetic analysis of coupled (or auxiliary) enzyme reactions. ChemRxiv, DOI: 10.26434/chemrxiv.5746065.
- Espenson, J. H., 1995. *Chemical Kinetics and Reaction Mechanisms*. McGraw-Hill, Singapore.
- Feng, S., Laketa, V., Stein, F., Rutkowska, A., MacNamara, A., Depner, S., Klingmüller, U., Saez-Rodriguez, J., Schultz, C., 2014. A rapidly reversible chemical dimerizer system to study lipid signaling in living cells. *Angew. Chem. Int. Ed.* 53, 6720–6723.
- Frenzen, C. L., Maini, P. K., 1988. Enzyme kinetics for a two-step enzymic reaction with comparable initial enzyme-substrate ratios. *J. Math. Biol.* 26, 689–703.
- Gallagher, R., 2004. Enzymes make the world go 'round. *Scientist* 18, 6.
- Hanson, S. M., Schnell, S., 2008. Reactant stationary approximation in enzyme kinetics. *J. Phys. Chem. A* 112, 8654–8658.
- Holmes, M. H., 2013. *Introduction to perturbation methods, second edition* Edition. Springer-Verlag, New York.

- Kuehn, C., 2015. Multiple time scale dynamics. Vol. 191 of Applied Mathematical Sciences. Springer-Verlag, New York.
- Letson, B., Rubin, J. E., Vo, T., 2017. Analysis of interacting local oscillation mechanisms in three-timescale systems. *SIAM J. Appl. Math.* 77, 1020–1046.
- Lin, C. C., Segel, L. A., 1988. Mathematics applied to deterministic problems in the natural sciences, 2nd Edition. Society for Industrial and Applied Mathematics (SIAM), Philadelphia, PA.
- Maini, P., Woolley, T., Baker, R., Gaffney, E., Seirin Lee, S., 2012. Turing’s model for biological pattern formation and the robustness problem. *Interface Focus* 2, 487–496.
- Murugan, R., 2018. Theory on the rate equation of Michaelis-Menten type single-substrate enzyme catalyzed reactions. *J. Math. Chem.* 56, 508–556.
- Nan, P., Wang, Y., Kirk, V., Rubin, J. E., 2015. Understanding and distinguishing three-time-scale oscillations: case study in a coupled Morris-Lecar system. *SIAM J. Appl. Dyn. Syst.* 14, 1518–1557.
- Roussel, M. R., Fraser, S. J., 1990. Geometry of the steady-state approximation: Perturbation and accelerated convergence methods. *J. Chem. Phys.* 93, 1072–1081.
- Roussel, M. R., Fraser, S. J., 1991. Accurate steady-state approximations: Implications for kinetics experiments and mechanism. *J. Phys. Chem.* 95, 8762–8770.
- Schnell, S., 2014. Validity of the Michaelis-Menten equation – Steady-state, or reactant stationary assumption: that is the question. *FEBS J.* 281, 464–472.
- Schnell, S., Maini, P. K., 2000. Enzyme kinetics at high enzyme concentration. *Bull. Math. Biol.* 62, 483–499.
- Schnell, S., Maini, P. K., 2002. Enzyme kinetics far from the standard quasi-steady-state and equilibrium approximations. *Math. Comput. Modelling* 35, 137–144.

- Schnell, S., Maini, P. K., 2003. A century of enzyme kinetics. Reliability of the  $K_M$  and  $v_{\max}$  estimates. *Comments Theor. Biol.* 8, 169–187.
- Schnell, S., Mendoza, C., 1997. Closed form solution for time-dependent enzyme kinetics. *J. Theor. Biol.* 187, 207–212.
- Segel, L. A., 1988. On the validity of the steady state assumption of enzyme kinetics. *Bull. Math. Biol.* 50, 579–593.
- Segel, L. A., Slemrod, M., 1989. The quasi-steady-state assumption: a case study in perturbation. *SIAM Rev.* 31, 446–477.
- Shoffner, S. K., Schnell, S., 2017. Approaches for the estimation of timescales in nonlinear dynamical systems: timescale separation in enzyme kinetics as a case study. *Math. Biosci.* 287, 122–129.
- Son, K. J., Shin, D.-S., Kwa, T., You, J., Gao, Y., Revzin, A., 2015. A microsystem integrating photodegradable hydrogel microstructures and reconfigurable microfluidics for single-cell analysis and retrieval. *Lab Chip* 15, 637–641.
- Vo, T., Bertram, R., Wechselberger, M., 2013. Multiple geometric viewpoints of mixed mode dynamics associated with pseudo-plateau bursting. *SIAM J. Appl. Dyn. Syst.* 12, 789–830.